ARMY RESEARCH LABORATORY

# Characterization of the Morphology of RDX Particles Formed by Laser Ablation

**by Jennifer L. Gottfried, Frank C. De Lucia Jr., and Stephanie M. Piraino**

**ARL-TR-5932** **February 2012**

## NOTICES

### Disclaimers

The findings in this report are not to be construed as an official Department of the Army position unless so designated by other authorized documents.

Citation of manufacturer's or trade names does not constitute an official endorsement or approval of the use thereof.

Destroy this report when it is no longer needed. Do not return it to the originator.

**Army Research Laboratory**
Aberdeen Proving Ground, MD 21005-5069

**ARL-TR-5932** **February 2012**

# Characterization of the Morphology of RDX Particles Formed by Laser Ablation

**Jennifer L. Gottfried, Frank C. De Lucia Jr., and Stephanie M. Piraino**
**Weapons and Materials Research Directorate, ARL**

| REPORT DOCUMENTATION PAGE | Form Approved OMB No. 0704-0188 |
|---|---|



| 1. REPORT DATE *(DD-MM-YYYY)* | 2. REPORT TYPE | 3. DATES COVERED (From - To) |
|---|---|---|
| February 2012 | Final | 1 October 2010–30 September 2011 |

**4. TITLE AND SUBTITLE**
Characterization of the Morphology of RDX Particles Formed by Laser Ablation

**5a. CONTRACT NUMBER**

**5b. GRANT NUMBER**

**5c. PROGRAM ELEMENT NUMBER**

**6. AUTHOR(S)**
Jennifer L. Gottfried, Frank C. De Lucia Jr., and Stephanie M. Piraino

**5d. PROJECT NUMBER**
AH80

**5e. TASK NUMBER**

**5f. WORK UNIT NUMBER**

**7. PERFORMING ORGANIZATION NAME(S) AND ADDRESS(ES)**
U.S. Army Research Laboratory
ATTN: RDRL-WML-A
Aberdeen Proving Ground, MD 21005-5069

**8. PERFORMING ORGANIZATION REPORT NUMBER**
ARL-TR-5932

**9. SPONSORING/MONITORING AGENCY NAME(S) AND ADDRESS(ES)**

**10. SPONSOR/MONITOR'S ACRONYM(S)**

**11. SPONSOR/MONITOR'S REPORT NUMBER(S)**

**12. DISTRIBUTION/AVAILABILITY STATEMENT**
Approved for public release; distribution is unlimited.

**13. SUPPLEMENTARY NOTES**

**14. ABSTRACT**
The morphology of cyclotrimethylenetrinitramine (RDX) particles produced by laser ablation has been characterized using scanning electron microscopy and Scanning Mobility Particle Sizer analyses. The effects of laser pulse energy, wavelength, and duration have been studied. Higher laser pulse energies resulted in higher concentrations of ablated RDX particles. Ultraviolet laser radiation is absorbed by RDX and results in the formation of agglomerated particles. Nano-RDX (mean particle size = 64 nm) was formed via near-infrared, nanosecond-pulsed laser ablation. Femtosecond laser ablation provides several advantages over nanosecond lasers because of the extremely high peak power and ultrashort time scale, but the increased experimental complexity may not be justified for this application.

**15. SUBJECT TERMS**
SEM, RDX morphology, laser ablation, nanoparticles

| 16. SECURITY CLASSIFICATION OF: | | | 17. LIMITATION OF ABSTRACT | 18. NUMBER OF PAGES | 19a. NAME OF RESPONSIBLE PERSON |
|---|---|---|---|---|---|
| a. REPORT | b. ABSTRACT | c. THIS PAGE | | | Jennifer L. Gottfried |
| Unclassified | Unclassified | Unclassified | UU | 28 | 19b. TELEPHONE NUMBER (*Include area code*) 410-278-7573 |

**Standard Form 298 (Rev. 8/98)**
Prescribed by ANSI Std. Z39.18

## Contents

## List of Figures

## List of Tables

## Acknowledgments

The authors wish to thank Melissa Meyer for performing the initial scanning electron microscopy analyses of ablated cyclotrimethylenetrinitramine (RDX) samples, Rose Pesce-Rodriguez for providing the research-grade RDX samples, and Kim Spangler for providing the pressed RDX samples (prepared by Roy Maulbetsch and Terry Piatt).

# 1. Introduction

Two of the primary goals in current energetic materials research are enhancing the performance and decreasing the sensitivity. In recent years it has been suggested that nanometer-scale particles would provide faster energy release, more complete combustion, and better control over material properties (*1–3*). In addition, studies have shown that the stability of cyclotrimethylenetrinitramine (RDX) crystals is affected by impurities, particle size, and sample preparation (*4*). It has also been demonstrated that decreasing the particle size decreases the mechanical and thermal sensitivity of RDX (*5–7*). The production of nano-RDX typically involves complicated experimental apparatus and/or difficulties in process scale-up, including sol-gel processing (*8*), aerosol jetting (*9, 10*), milling (*11*), rapid expansion of a supercritical solution (*7, 12*), and spray drying (*13*).

Laser ablation provides a convenient tool for producing nanoparticles of a wide variety of materials, but predicting particle size, formation rates, and degree of aggregation from first principles is not yet possible (*14*). Metallic nanoparticle formation by laser ablation has been studied by several groups and has been demonstrated to be dependent on laser pulse energy, duration, and wavelength (*15–18*). Femtosecond lasers have been used to machine energetic materials for over a decade (*19, 20*), and several recent studies have investigated the resulting ionized fragment/cluster products using mass spectrometry (*21, 22*). To our knowledge, however, no one has characterized the morphology of laser-ablated energetic materials. The objective of this research was to produce and characterize the solid products produced from laser ablation of RDX, including nanoparticles, under a range of experimental conditions. Characterization of the products produced by laser ablation of RDX would also benefit applications such as the detection of explosives with laser-induced breakdown spectroscopy (LIBS) (*23*) and studies of the laser-induced plasma chemistry of RDX (*24, 25*).

Two approaches to characterizing the ablated RDX were developed: (1) imaging analysis of particles collected on a glass slide and (2) particle size analysis via direct sampling of the ablated material. Scanning electron microscopy (SEM) was used to image the ablated particles; however, at higher magnifications, damage to the RDX crystals from the electron beam was observed so only micron-scale information about the particle morphology could be inferred from this technique. The Scanning Mobility Particle Sizer (SMPS) was used to measure the size distribution of the ablated particles in the size range from 10 to 400 nm. Together, these techniques enabled us to determine the effect of the laser pulse energy, wavelength, and duration.

## 2. Experimental Method

### 2.1 Materials

The energetic materials studied included an M43 propellant grain that consists of ~76% RDX, 12% cellulose acetate butyrate (CAB), 8% plasticizer, and 4% nitrocellulose (NC) (*26*). Class-1 (<850 μm) and class-5 (<45 μm) military-grade and research-grade (i.e., purified to remove cyclotetramethylene tetranitramine, HMX) RDX powders were obtained from colleagues at the U.S. Army Research Laboratory (ARL). Pressed RDX pellets (5-mm diameter, 2.5-mm width) were prepared from a 75% class-1 and 25% class-5 mixture of military-grade RDX; the samples were wet in methanol and pressed to ~95% theoretical maximum density (TMD).

### 2.2 Lasers

For the laser ablation of the RDX samples, the lasers in each experimental setup were focused onto the sample surface using a 10-cm focal length lens. The lasers used in the study included an Nd:YAG Big Sky CFR200 laser (1064 nm, 12 ns) at 8, 75, and 200 mJ; an Nd:YAG Quantel Brilliant B laser with a third harmonic generator (355 nm, 5 ns) at 30 and 180 mJ; and a Ti:sapphire amplifier (Coherent Hidra-25) seeded by a femtosecond-pulsed oscillator (Coherent Vitesse, 800 nm, 100 fs). A Nd:YLF pump laser (Coherent Evolution-15) amplified the output energy of the femtosecond laser to ~1 mJ, and an Nd:YAG pump laser (Continuum Powerlite Precision II 8000) further amplified the femtosecond pulse energy to ~20 mJ. Femtosecond pulses at 900 μJ and 7 mJ were used to ablate the RDX samples. For each of the experimental configurations, a laser-induced plasma lasting for hundreds of microseconds and consisting of highly excited atoms, ions, and free electrons was formed above the sample surface by the interaction of the laser with the RDX. The shock wave from the focused laser pulse also resulted in the dispersion of ablated particles above the sample surface, primarily along the vertical axis (i.e., opposite the direction of the laser propagation). The short duration of the pulsed lasers used in this work (<12 ns) was not sufficient to detonate any of the RDX samples.

### 2.3 SEM Analysis

Round microscope cover glasses (no. 2, 12-mm diameter) were placed above the laser focus to collect the ejected particles (figure 1). Since the 355-nm laser was absorbed by the glass, the slide was held at an angle adjacent to the laser-induced plasma for those experiments. Multiple laser pulses (~5–100) were required to obtain sufficient surface coverage on the glass slides. In general, samples in pelletized form and lasers with higher pulse energy required fewer laser pulses. For comparison to the ablated samples, unablated samples of RDX were prepared directly for SEM analysis. The RDX powder was simply transferred to the surface of an aluminum stud for analysis, while the RDX pellet samples were scraped off the pellet surface with a metal spatula.

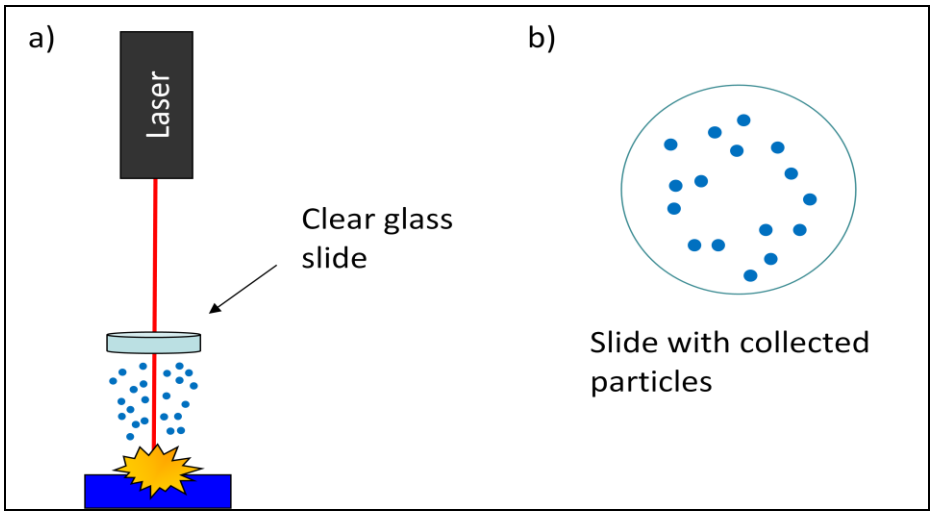


Figure 1. (a) Experimental setup for collection of laser-ablated particles and (b) the glass cover slide with the collected particles for SEM analysis.

An ISI-SS40 scanning electron microscope was used to analyze the RDX samples. The glass slides were mounted on conductive (aluminum) studs using a conductive adhesive. The samples were coated with a thin conductive film via "cold sputtering" (*27*). The sample was placed in the instrument chamber, and a vacuum was applied. Various images were taken using different working distances and voltages to determine the optimum image quality. The working distance was set at 20 mm, and the voltage was 10 kV (except where noted). Images were taken at approximate magnifications ranging from 150× to 6000×.

### 2.4 SMPS Analysis

Direct sampling of the aerosolized stream of ablated particles was achieved with a custom-built sample chamber and a particle size analyzer (figure 2). The 5-cm-diameter aluminum sample chamber was designed with a 2-mm-diameter inlet and a 4-mm-diameter outlet to carry the stream of aerosolized particles to the particle sizer. A sapphire window, which is transparent to the laser wavelengths, sealed the sample chamber. Because the intake on the particle sizer was under vacuum, the inlet on the sample chamber was left open to the atmosphere (although a carrier gas could be used in future experiments to influence the size or composition of the ablated particles). When a sheath flow rate of 6 liters per minute (lpm) and a sample flow rate of 0.6 lpm were used, the aerosolized particles were carried into the SMPS (TSI model 3936), where the electrostatic classifier (TSI model 3080) charged the particles to a known charge distribution and classified them according to their ability to traverse an electrical field in a differential mobility analyzer (TSI model 3081). A condensation particle counter (TSI model 3010) counted the particles based on a laser light-scattering technique. With our setup, the software enables scanning of particle sizes from 10 to 400 nm in 135 s. The laser was fired continuously at 1 Hz for these measurements.

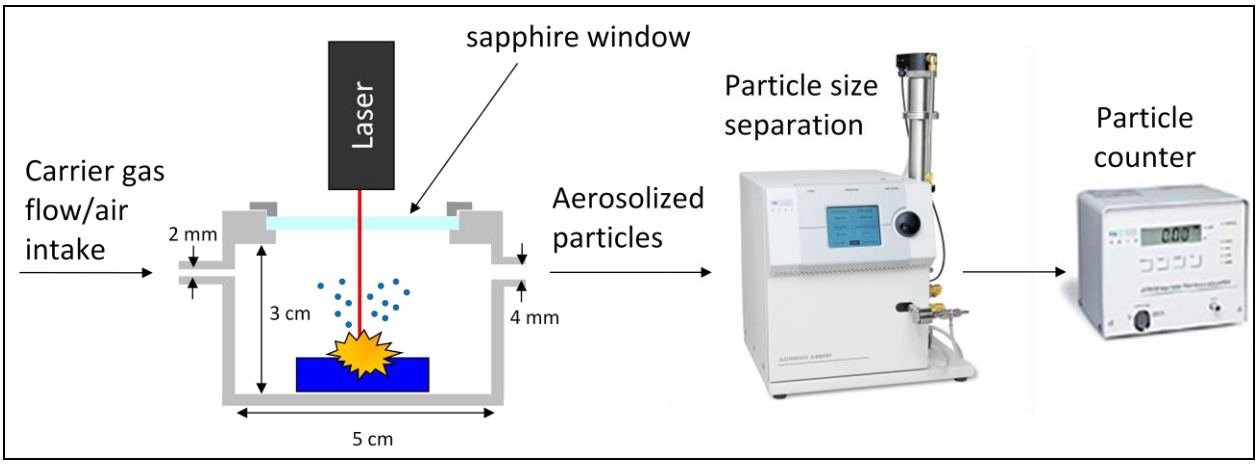


Figure 2. Experimental setup for in situ measurement of laser-ablated particle sizes.

## 3. Results and Discussion

### 3.1 Survey of RDX Samples

SEM analysis of the M43 propellant grain ablated by 200 mJ at 1064 nm showed that significant melting of the binder (inert CAB polymer) occurred (figure 3). Because of the difficulty in discriminating between RDX and the other components of the propellant, we decided to use only RDX samples.

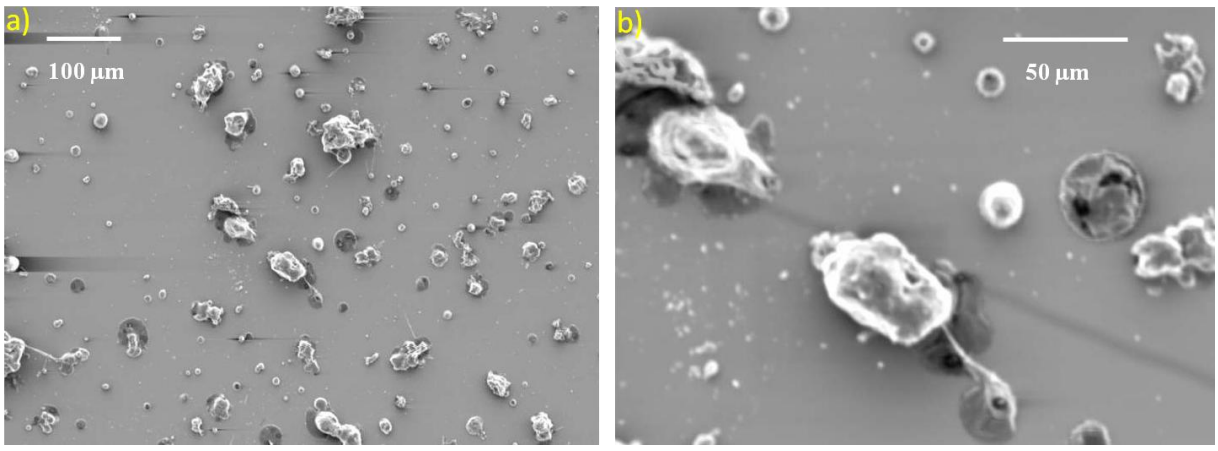


Figure 3. SEM images of laser-ablated M43 propellant grain at (a) 150× magnification and (b) 500× magnification (working distance: 40 mm; voltage: 5 kV).

Figures 4 and 5 show the SEM images from pure, unablated research-grade RDX (class-1 and class-5 particle sizes, respectively). Damage to the crystal surface from the electron beam (pitting and cracking) becomes visible at higher magnifications for the larger-grade RDX.

Unfortunately, we were unable to obtain SEM images of the ablated research-grade samples because the shock wave from the ablation laser dispersed the loose powder too much. Although the loose RDX could be affixed to double-sided sticky tape to improve the ablation efficiency, small amounts of the tape would also be ablated. The SEM images of the unablated research-grade RDX are included here for documentation purposes.

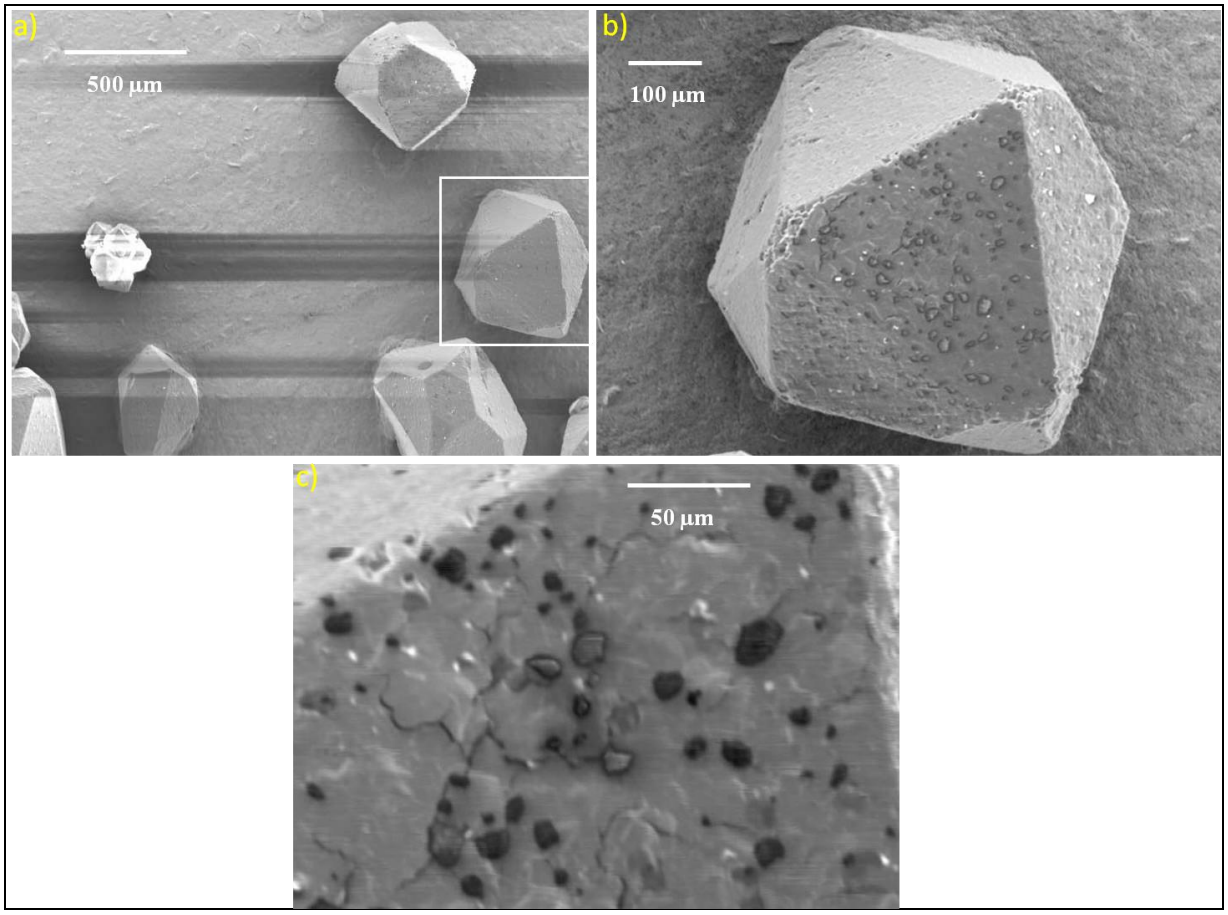


Figure 4. SEM images of unablated research-grade class-1 RDX at (a) 50× magnification, (b) 150× magnification, and (c) 500× magnification (working distance: 40 mm; voltage: 5 kV).

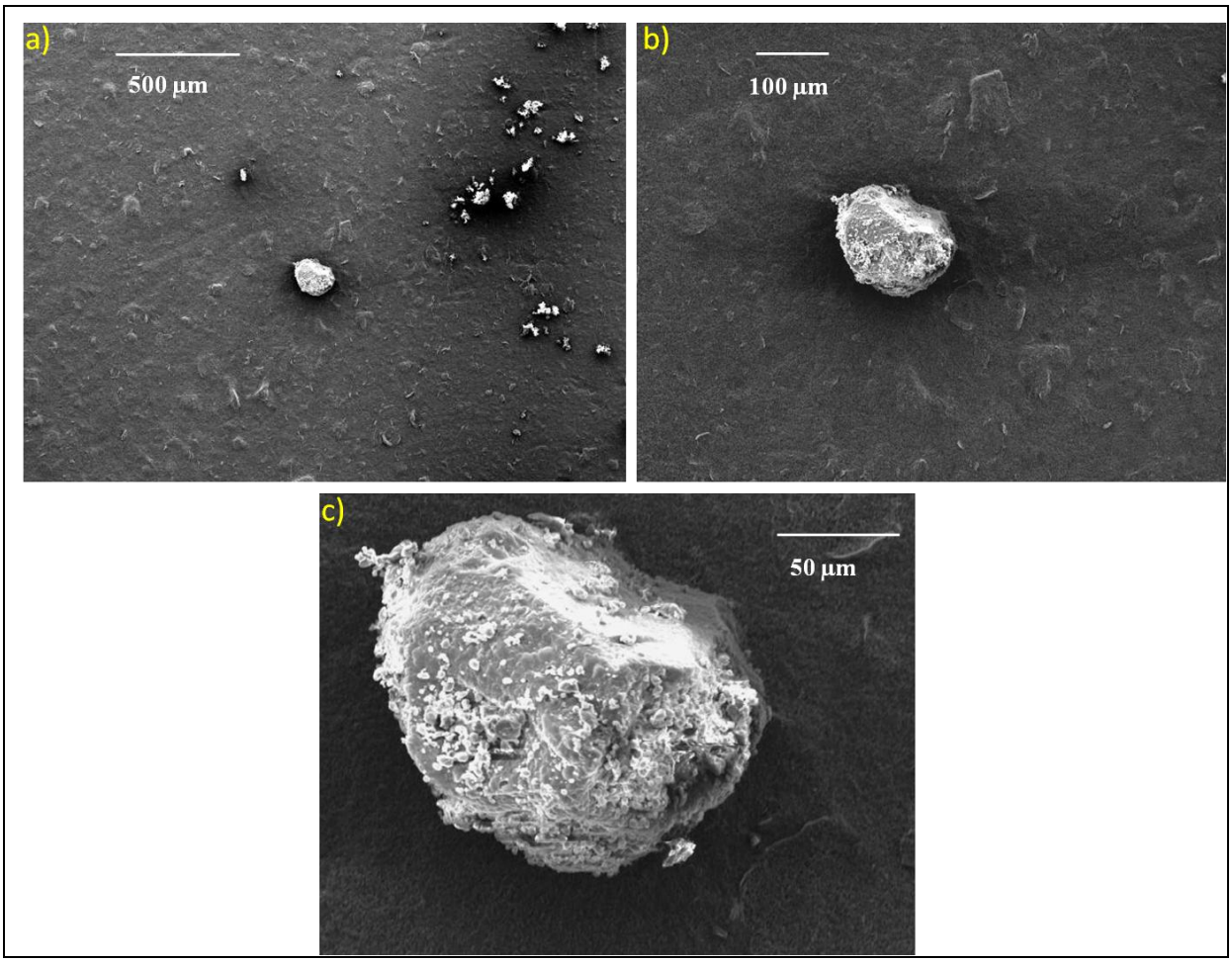


Figure 5. SEM images of unablated research-grade class-5 RDX at (a) 50× magnification, (b) 150× magnification, and (c) 500× magnification.

Pressed RDX pellets with no binders or fillers were subsequently prepared to provide good starting material for the laser ablation experiments. Because military-grade class-1 and class-5 RDX was used to prepare the pressed pellets, we also obtained SEM images of the unpressed military-grade RDX powders (figures 6 and 7). Unlike research-grade RDX, military-grade RDX can contain significant amounts of HMX (up to 5% for type-I RDX produced by direct nitration with the Woolwich process and up to 17% for type-II RDX produced by an acetic anhydride Bachmann process) (*28*). Once ablated, SEM cannot differentiate between RDX particles and HMX particles, although a Fourier transform infrared microscope could be used to differentiate the particles. The morphology of the military-grade RDX samples is quite different from the research-grade RDX. Unfortunately, no information about the processing or treatment of the provided RDX samples was available.

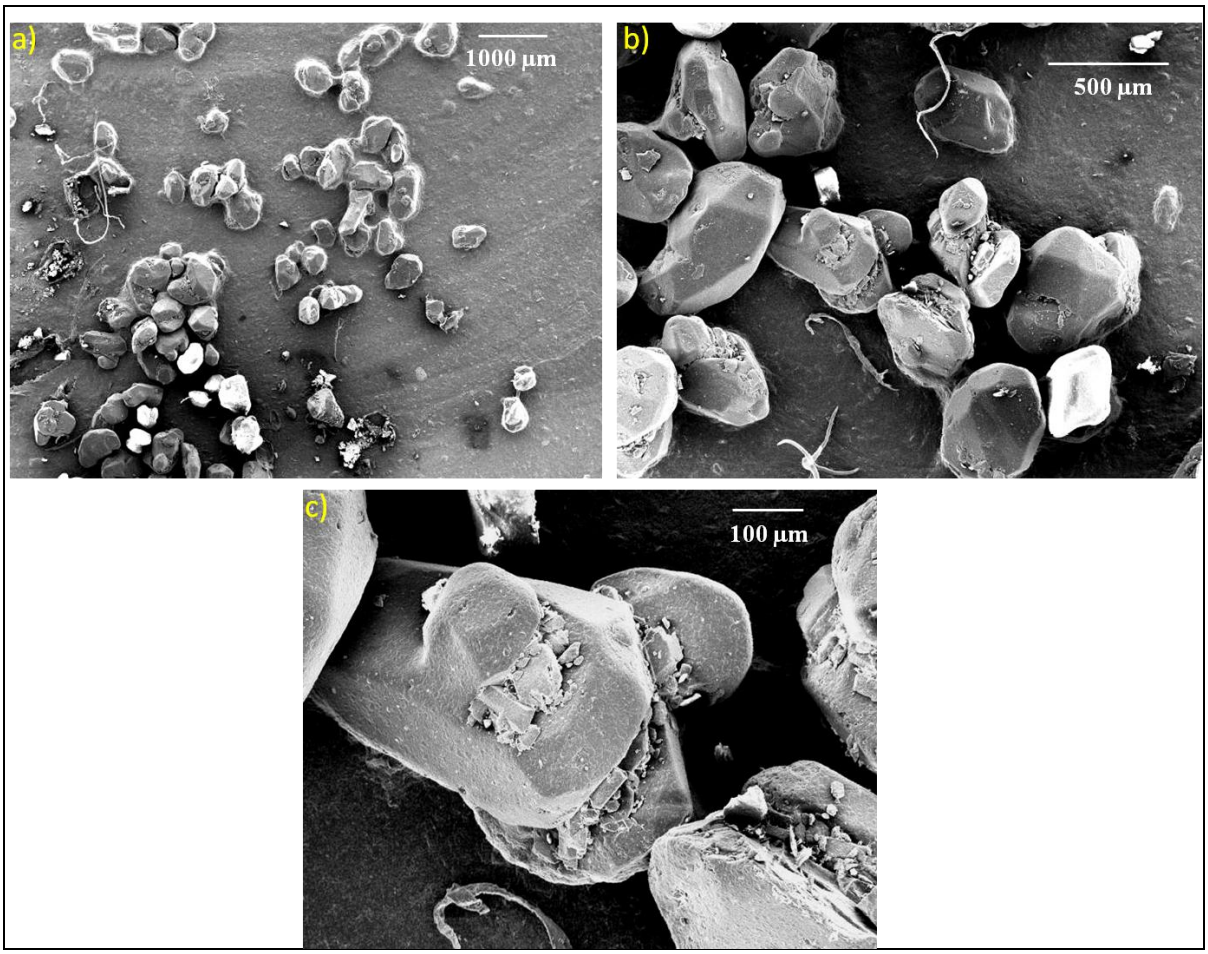


Figure 6. SEM images of unablated, unpressed military-grade class-1 RDX at (a) 14× magnification, (b) 50× magnification, and (c) 150× magnification.

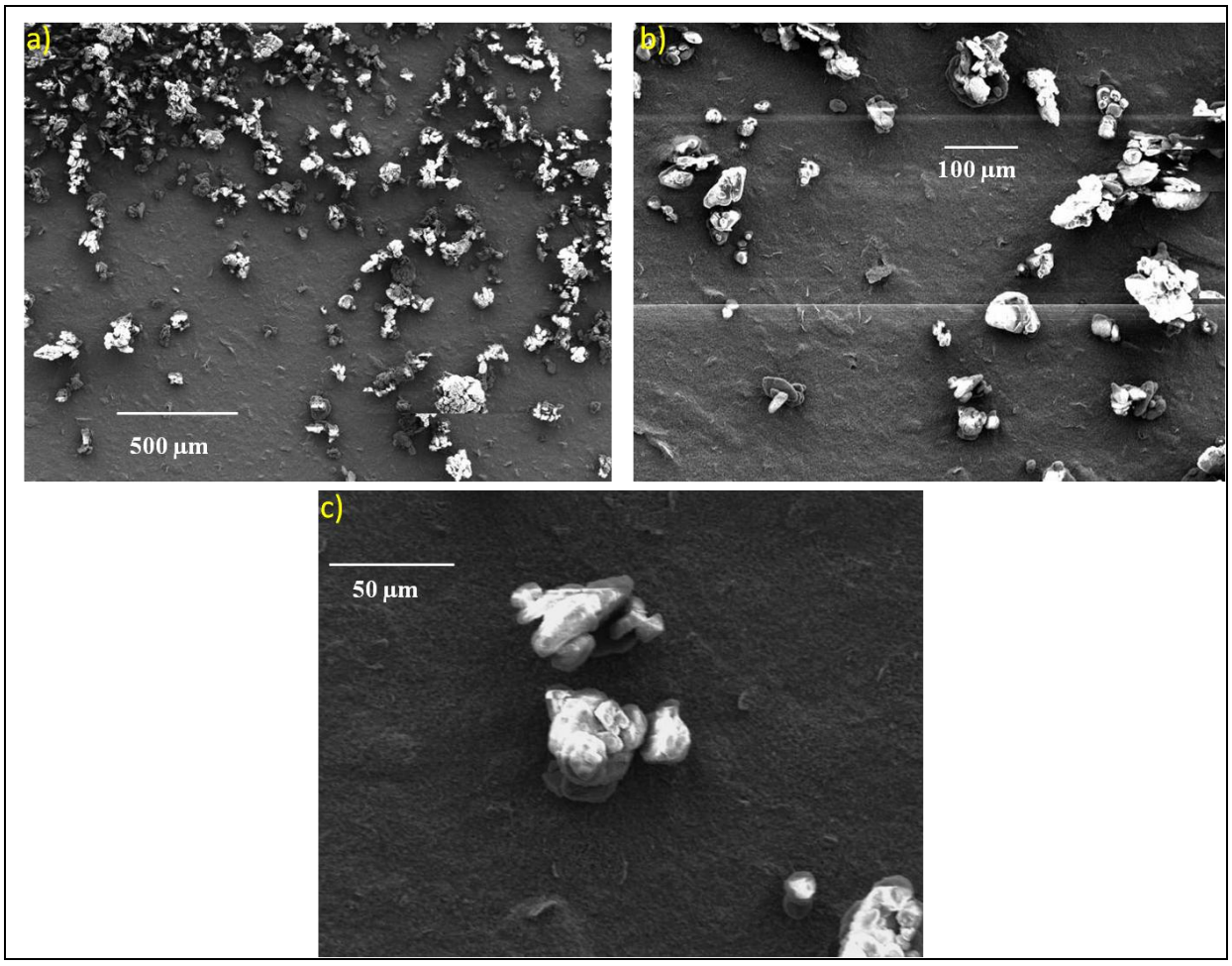


Figure 7. SEM images of unablated, unpressed military-grade class-5 RDX at (a) 50× magnification, (b) 150× magnification, and (c) 500× magnification.

As shown in figure 8, the class-1 and class-5 military-grade RDX particle sizes (originally <850 and <45 µm, respectively [*28*]) are significantly reduced after being pressed. Based on the wide-field view of the distribution of the two particle sizes after being pressed into the pellet at $3.3 \times 10^4$ lb/in$^2$ (figure 8a), it appears that figure 8b is a crystal of class-1 RDX that has been compressed in size by an order of magnitude or more. The confinement of the RDX in pellet form significantly reduced the number of laser pulses needed to ablate a sufficient amount of material for analysis and prevented the need to move the RDX sample after each laser shot. The analyses described in the following sections were based on ablation of the pressed military-grade RDX samples.

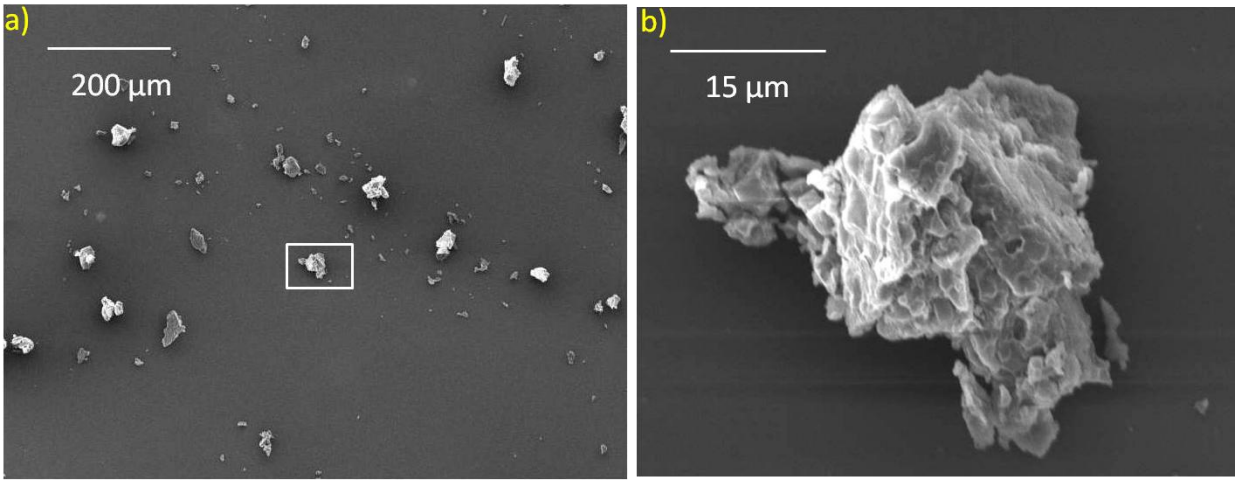


Figure 8. SEM images of unablated, pressed military-grade RDX (75% class 1, 25% class 5) at (a) 120× magnification and (b) 2000× magnification.

### 3.2 SEM Analysis of Laser-Ablated RDX

Laser ablation (1064 nm) of the pressed military-grade RDX sample resulted in smaller, more spherical RDX particles compared to the unablated particles shown in figure 8 (figure 9). Higher laser pulse energy (200 mJ, compared to 75 mJ) produced significantly more submicron particles. Absorption of the incident laser in the laser-induced plasma scales with the square of the wavelength (*29*). Thus, when near-infrared wavelengths (1064 nm) are used, the coupling of the laser to the solid surface is reduced since more of the incident laser light will be absorbed by the laser-induced plasma (i.e., plasma shielding effect). On the other hand, more of the ultraviolet (UV) laser (355 nm) will reach the sample surface since it is not as strongly absorbed by the plasma. Figure 10 shows the SEM images from the laser ablation of RDX at 355 nm. Most energetic materials do not absorb near-infrared or visible light, but the UV laser is strongly absorbed by the RDX (*30*). Ablation with only 30 mJ of UV laser energy was not very efficient—relatively few particles were collected on the glass slide. At the higher UV laser energy (180 mJ), however, an agglomeration of smaller particles was observed. The RDX-ablated particles appear to be almost melted together. These agglomerated RDX particles were easily damaged by an electron beam, even at lower magnifications.

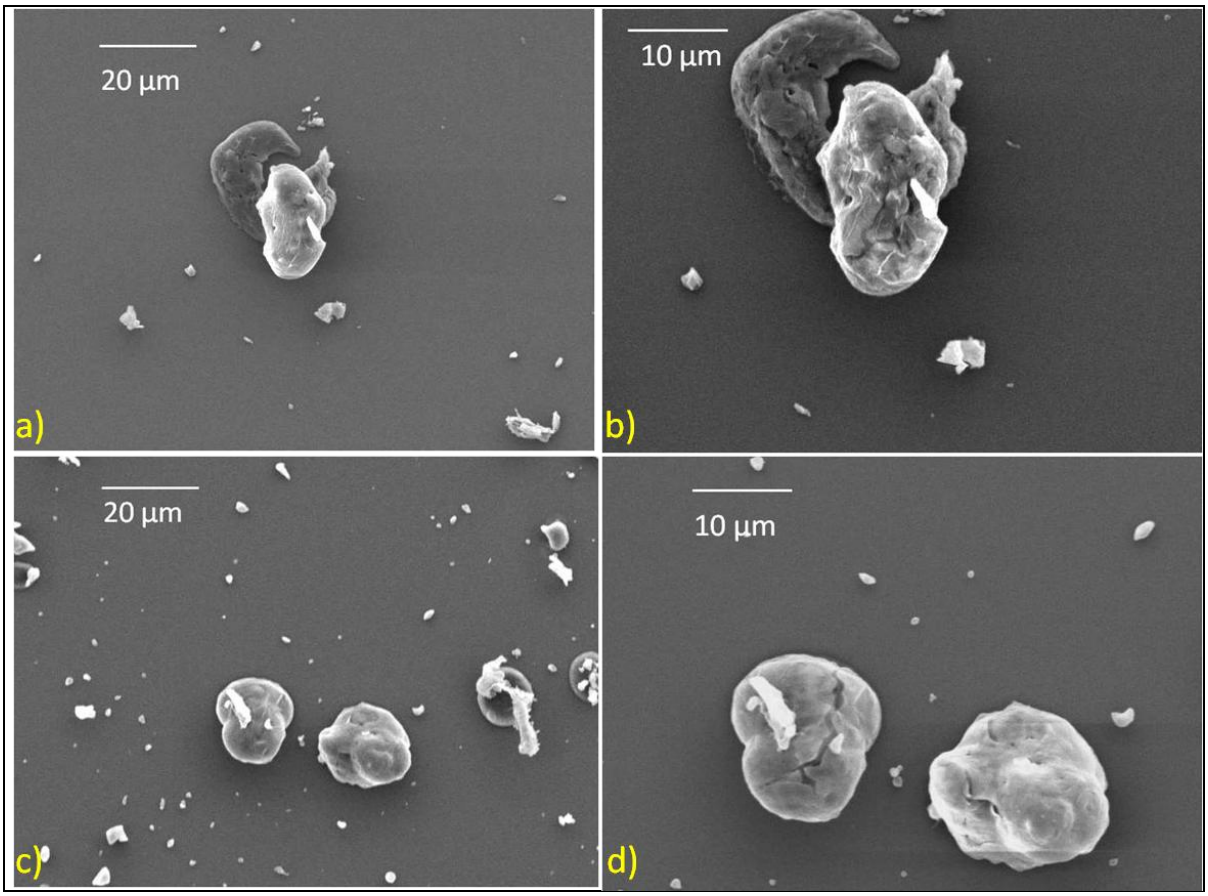


Figure 9. SEM images of pressed military-grade RDX ablated with a 1064-nm laser at 75 mJ: (a) 1000× magnification and (b) 2000× magnification, and at 200 mJ: (c) 1000× magnification and (d) 2000× magnification.

Because it is desirable to have minimal thermal and mechanical effects during the production of nano-RDX, the ablation process should ideally be accomplished without coupling laser energy into the energetic material. For nanosecond laser pulses, damage to the surrounding material occurs via thermal deposition, resulting in melting and boiling of the energetic material. Ablation of the RDX with a femtosecond laser presents a distinct advantage over nanosecond-pulsed ablation. The time scale for the absorption of the femtosecond pulse is so short that the energetic material is ablated with very little heat transfer to the surrounding material. For this reason, femtosecond lasers have been used for cutting and machining energetic materials (*19*, *20*). A 2003 paper by Roeske et al. (*3*, *20*) showed that the surfaces of the cut energetic materials were undamaged, but they did not analyze the ablated material. Figure 11 shows the SEM images for the RDX particles ablated by the femtosecond laser at low (900 µJ) and high (7 mJ) pulse energies. Unlike the 1064-nm nanosecond laser ablation (figure 9), the femtosecond laser appears to produce a narrower size distribution of particles and agglomerated material, especially at 7 mJ. A comparison of the SEM images for the low- and high-energy femtosecond laser pulses showed that the average particle size decreased about 28% (from 3.00 to 2.17 µm in diameter) for the 7-mJ laser pulse compared to the 900-µJ pulse.

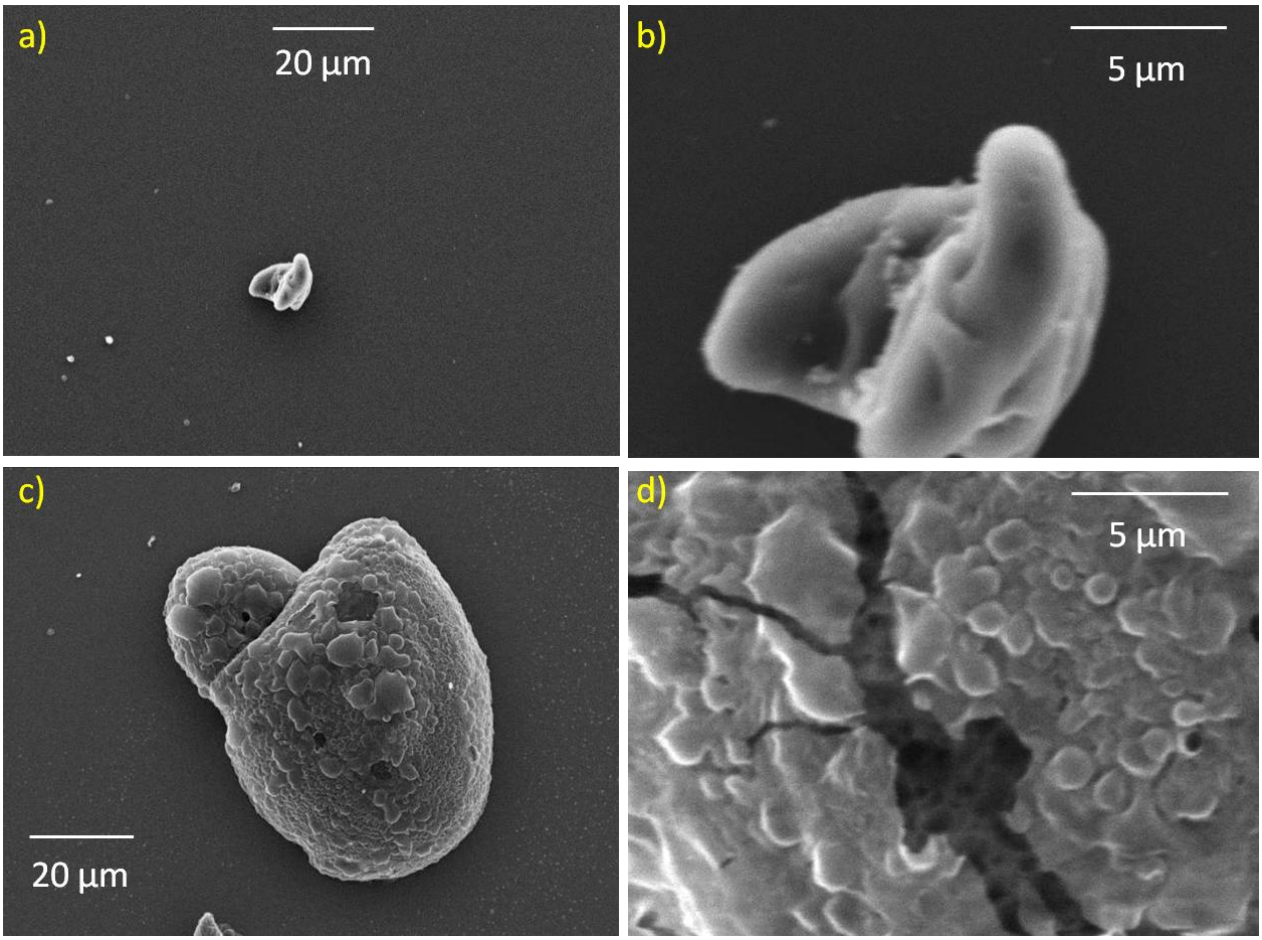


Figure 10. SEM images of pressed military-grade RDX ablated with a 355-nm laser at 30 mJ: (a) 1000× magnification and (b) 6000× magnification, and at 180 mJ: (c) 1000× magnification and (d) 6000× magnification.

### 3.3 SMPS Analysis of Laser-Ablated RDX

In addition to the SEM analysis of the micron-scale features of the ablated RDX, the nanoparticle size distribution of the ablated RDX was measured with the SMPS instrument. Near-infrared, nanosecond pulsed laser ablation of the pressed RDX pellet was compared at three different laser energies (8, 75, and 100 mJ). As seen in figure 12, the 200-mJ pulse produced the highest concentration of nano-RDX, although the 75-mJ pulse produced a similar particle size distribution. The mean particle size was ~64 nm for both energies, with a mode (i.e., the particle size that occurs most frequently in the distribution) of ~50 nm. The 8-mJ laser pulse produced the lowest concentration of nano-RDX, and the distribution was skewed to larger particle sizes (~86 nm). Table 1 summarizes the statistics for the particle size results (three separate measurements at 75 mJ were averaged together).

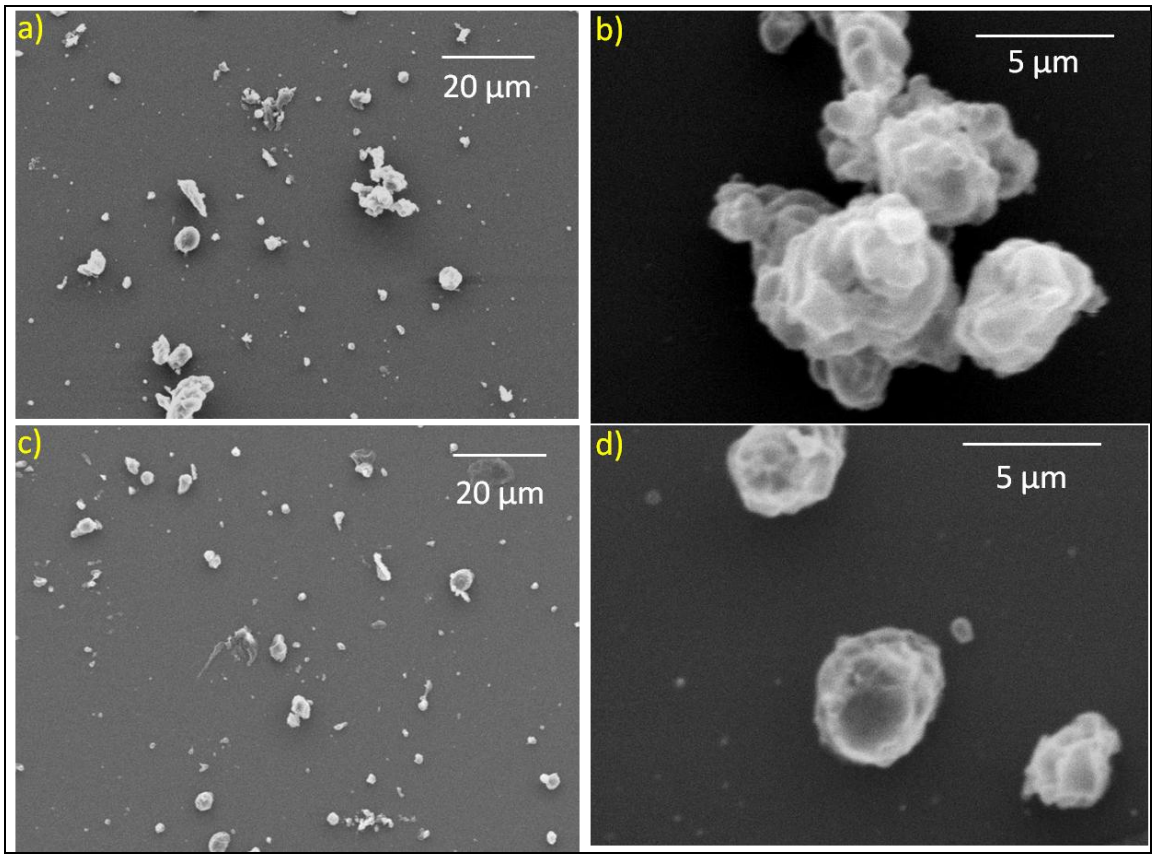


Figure 11. SEM images of pressed military-grade RDX ablated with a 100-fs laser pulse (800 nm) at 900 µJ: (a) 1000× magnification and (b) 6000× magnification, and at 7 mJ: (c) 1000× magnification and (d) 6000× magnification.

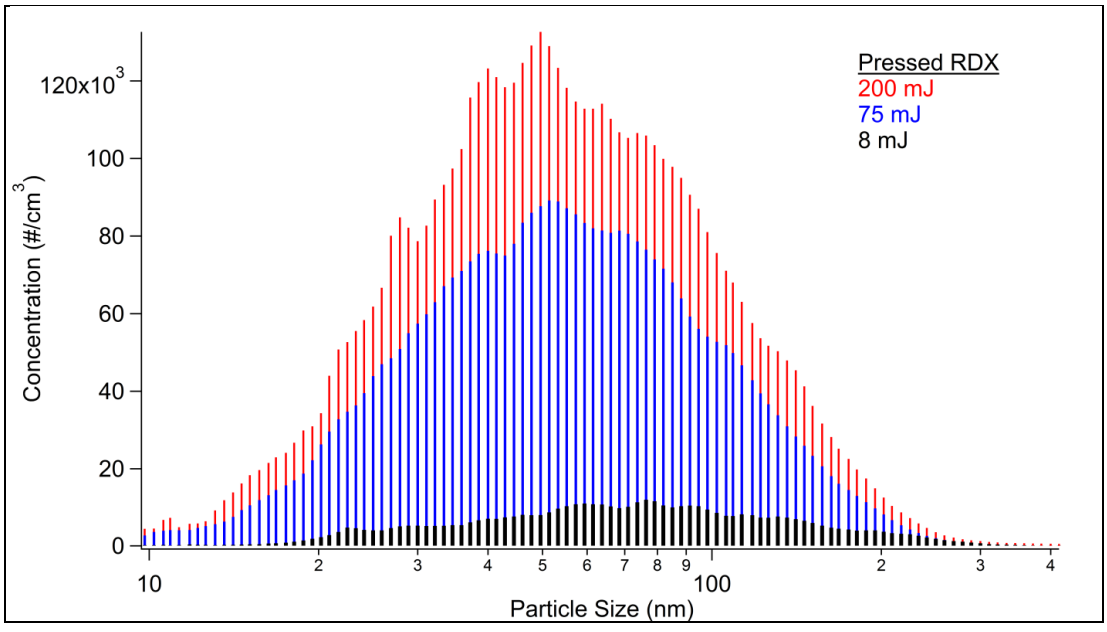


Figure 12. Histogram of particle sizes produced using three different laser ablation energies on the pressed military-grade RDX.

Table 1. Statistics for RDX particles produced by three different laser ablation energies (10- to 400-nm particle sizes measured). (From data in figures 12 and 13.)

| Laser Energy (mJ) | Mean (nm) | Mode (nm) | Total Concentration (#/cm$^3$) |
|---|---|---|---|
| 8 | 85.7 | 76.4 | $5.06 \times 10^5$ |
| 75 | 64.2 ± 2.6 | 50.8 ± 2.8 | $3.78 \pm 0.28 \times 10^6$ |
| 75[a] | 91.9 | 61.5 | $1.38 \times 10^7$ |
| 200 | 64.3 | 49.6 | $5.52 \times 10^6$ |

[a]Laser focus lowered into RDX pellet.

In addition to laser pulse energy, wavelength, and pulse duration, another important experimental parameter to consider is the position of the laser focus. Increasing the height of the RDX pellet relative to the laser focus increased the number of RDX particles produced but also skewed the distribution of ablated particles to larger sizes (figure 13). Lowering the laser focus into the center of the pellet, rather than on the surface, decreases the laser fluence (energy density) at the surface and prevents air breakdown above the sample surface. Air breakdown results in a distortion of the laser beam and loss of ablation energy.

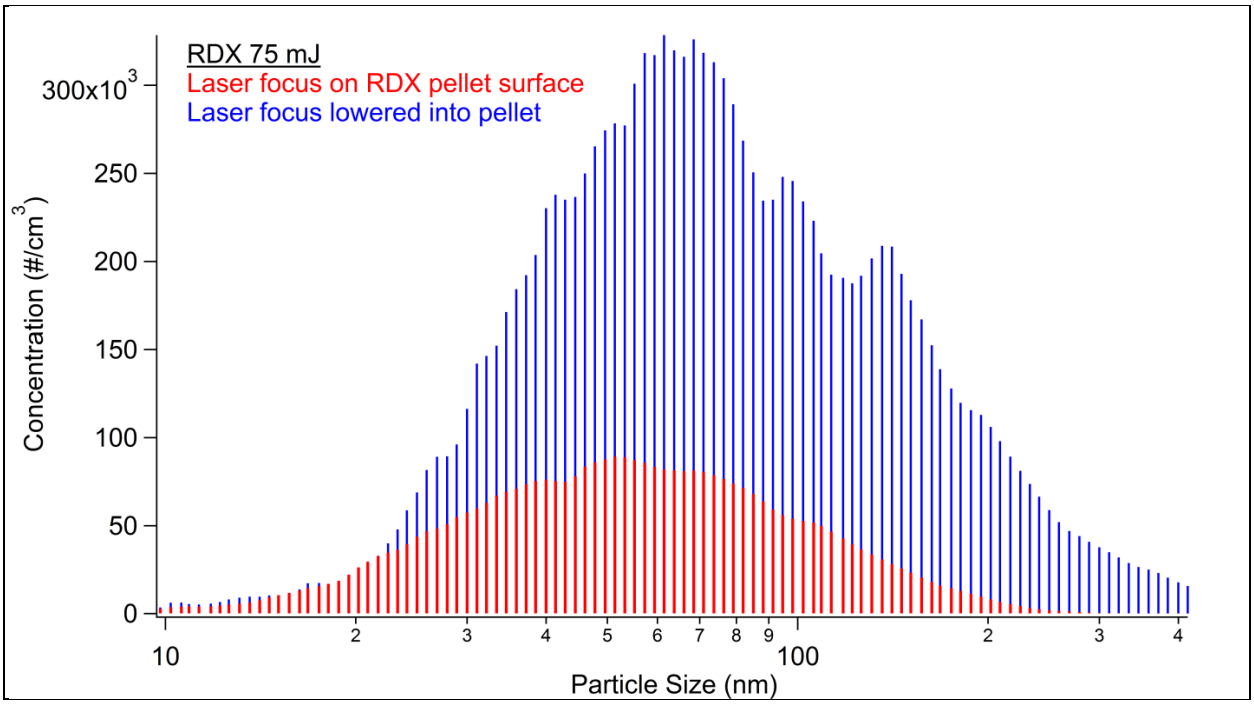


Figure 13. Comparison of particle size distributions as a function of laser focus position relative to the pressed military-grade RDX pellet surface.

## 4. Conclusions

We have successfully demonstrated, for the first time, the production of nano-RDX particles (~64 nm) via laser ablation. In addition, the effects of laser pulse energy, wavelength, and duration on the ablated RDX have been studied. In general, higher-energy laser pulses produce a larger concentration of ablated particles since more mass is removed from the sample with each laser pulse. UV laser ablation of RDX results in the formation of agglomerated RDX particles because more of the laser energy is absorbed by the RDX. Femtosecond laser ablation efficiently removes the RDX with minimal damage to the surrounding material. While the femtosecond laser appears to produce smaller (agglomerated) particle sizes on the micron scale, we could not perform SMPS analysis of the femtosecond ablation because the sapphire window on the sample chamber converts the light from the femtosecond pulse to a "white-light continuum" or "supercontinuum." The sapphire window was chosen because of its high transmittance over a broad wavelength range; however, when a femtosecond pulse is focused through a transparent medium, nonlinear effects give rise to extreme spectral broadening (*31*). Because of the increased experimental complexity resulting from the use of femtosecond laser pulses, it may be more advantageous to use the near-infrared nanosecond laser for ablation of RDX particles.

Ultimately, the technique demonstrated here could be used to study the chemistry and mechanical properties of nano-RDX. The differential mobility analyzer on the particle sizer can be used to produce an aerosolized stream of uniformly sized nano-RDX particles for further experimental studies. By controlling the experimental parameters for laser ablation of RDX, we could potentially produce RDX particles with specific morphologies in support of microstructural experiments for the Multiscale Response of Energetic Materials mission program.

## 5. References


1. Brousseau, P.; Anderson, C. J. Nanometric Aluminum in Explosives. *Propellants Explos. Pyrotech.* **2002**, *27* (5), 300–306.
2. Yang, Y. Q.; Sun, Z. Y.; Wang, S. F.; Dlott, D. D. Fast Spectroscopy of Laser-Initiated Nanoenergetic Materials. *J. Phys. Chem. B* **2003**, *107* (19), 4485–4493.
3. Dlott, D. D. Thinking Big (and Small) About Energetic Materials. *Mater. Sci. Technol.* **2006**, *22*, 463–473.
4. Erofeev, L. N.; Tarasov, Y. P.; Kalmykov, Y. B.; Shu, Y.; Dubikhin, V. V.; Nazin, G. M. Crystal Defects and Stability of RDX. *Russ. Chem. Bull.* **2001**, *50* (6), 1000–1002.
5. Song, X.-I.; Li, F.-S.; Zhang, J.-L.; Guo, X.-D.; An, C.-W.; Wang, Y. Influence of Particle Size, Morphology and Size Distribution on the Safety and Thermal Decomposition Properties of RDX. *J. Solid Rocket Technol.* **2008**, *31* (2), 168–172.
6. Song, X. L.; Li, F. S. Dependence of Particle Size and Size Distribution on Mechanical Sensitivity and Thermal Stability of Hexahydro-1, 3, 5-trinitro-1, 3, 5-triazine. *Def. Sci. J.* **2009**, *59* (1), 37–42.
7. Stepanov, V.; Anglade, V.; Balas Hummers, W. A.; Bezmelnitsyn, A. V.; Krasnoperov, L. N. Production and Sensitivity Evaluation of Nanocrystalline RDX-Based Explosive Compositions. *Propellants Explos. Pyrotech.* **2011**, *36*, 240–246.
8. Tillotson, T. M.; Hrubesh, L. W.; Simpson, R. L.; Lee, R. S.; Swansiger, R. W.; Simpson, L. R. Sol-Gel Processing of Energetic Materials. *J. Non-Cryst. Solids* **1998**, *225* (0), 358–363.
9. Mercado, L.; Torres, P. M.; Gomez, L. M.; Mina, N.; Hernandez, S. P.; Lareau, R.; Chamberlain, R. T.; Castro-Rosario, M. E. Synthesis and Characterization of High-Energy Nanoparticles. *J. Phys. Chem. B* **2004**, *108* (33), 12314–12317.
10. Spitzer, D.; Baras, C.; Schäfer, M. R.; Ciszek, F.; Siegert, B. Continuous Crystallization of Submicrometer Energetic Compounds. *Propellants Explos. Pyrotech.* **2011**, *36* (1), 65–74.
11. Redner, P.; Kapoor, D.; Patel, R.; Chung, M.; Martin, D. Production and Characterization of Nano-RDX; U.S. Army Armament Research, Development, and Engineering Center: Picatinny, NJ, 2006.
12. Cortopassi, A. C.; Kuo, K. K.; Ferrara, P. J. Synthesis of Nano-Sized RDX Using an Ultra-High Pressure Ress System. *Int. J. Energ. Mater. Chem. Propuls.* **2008**, *7* (1), 39–5454.

13. Qiu, H.; Stepanov, V.; Stasio, A. R. D.; Chou, T.; Lee, W. Y. RDX-Based Nanocomposite Microparticles for Significantly Reduced Shock Sensitivity. *J. Hazard. Mater.* **2011**, *185*, 489–493.

14. Hergenröder, R. Laser-Generated Aerosols in Laser Ablation for Inductively Coupled Plasma Spectrometry. *Spectrochim. Acta, Part B* **2006**, *61* (3), 284–300.

15. Ullmann, M.; Friedlander, S. K.; Schmidt-Ott, A. Nanoparticle Formation by Laser Ablation. *J. Nano. Res.* **2002**, *4* (6), 499–509.

16. Amoruso, S.; Bruzzese, R.; Wang, X.; Ausanio, G.; Lanotte, L. Laser-Induced Modification of the Size Distribution of Nanoparticles Produced During Ultrashort Laser Ablation of Solid Targets in Vacuum. *J. Phys. B* **2007**, *40* (6), 1253–1258.

17. Eliezer, S.; Eliaz, N.; Grossman, E.; Fisher, D.; Gouzman, I.; Henis, Z.; Pecker, S.; Horovitz, Y.; Fraenkel, M.; Maman, S.; Lereah, Y. Synthesis of Nanoparticles With Femtosecond Laser Pulses. *Phys. Rev. B* **2004**, *69* (14), 144119.

18. Sattari, R.; Dieling, C.; Barcikowski, S.; Chichkov, B. Laser-Based Fragmentation of Microparticles for Nanoparticle Generation. *J. Laser Micro. Nanoengineer.* **2008**, *3* (2), 100–105.

19. Perry, M. D.; Stuart, B. C.; Banks, P. S.; Feit, M. D.; Yanovsky, V.; Rubenchik, A. M. Ultrashort-Pulse Laser Machining of Dielectric Materials. *J. Appl. Phys.* **1999**, *85* (9), 6803–6810.

20. Roeske, F.; Benterou, J.; Lee, R.; Roos, E. Cutting and Machining Energetic Materials With a Femtosecond Laser. *Propellants, Explos., Pyrotech.* **2003**, *28* (2), 53–57.

21. McEnnis, C.; Dikmelik, Y.; Spicer, J. B. Femtosecond Laser-Induced Fragmentation and Cluster Formation Studies of Solid Phase Trinitrotoluene Using Time-of-Flight Mass Spectrometry. *Appl. Surf. Sci.* **2007**, *254* (2), 557–562.

22. Sovova, K.; Dryahina, K.; Spanel, P.; Kyncl, M.; Civis, S. A Study of the Composition of the Products of Laser-Induced Breakdown of Hexogen, Octogen, Pentrite and Trinitrotoluene Using Selected Ion Flow Tube Mass Spectrometry and Uv-Vis Spectrometry. *Analyst* **2010**, *135* (5), 1106–1114.

23. Gottfried, J. L.; De Lucia, F. C., Jr.; Munson, C. A.; Miziolek, A. W. Laser-Induced Breakdown Spectroscopy for Detection of Explosives Residues: A Review of Recent Advances, Challenges, and Future Prospects. *Anal. Bioanal. Chem.* **2009**, *395*, 283–300.

24. Babushok, V. I.; DeLucia, F. C.; Dagdigian, P. J.; Gottfried, J. L.; Munson, C. A.; Nusca, M. J.; Miziolek, A. W. Kinetic Modeling Study of the Laser-Induced Plasma Plume of Cyclotrimethylenetrinitramine (RDX). *Spectrochim. Acta, Part B* **2007**, *62* (12), 1321–1328.

25. Gottfried, J. L. Laser-Induced Plasma Chemistry of the Explosive RDX With Various Metallic Nanoparticles. *Appl. Opt.* **2012**, in press.

26. McNesby, K. L.; Wolfe, J. E.; Morris, J. B.; Pesce-Rodriguez, R. A. *FT-Raman Spectroscopy of Some Energetic Materials and Propellant Formulations*; ARL-TR-233; U.S. Army Research Laboratory: Aberdeen Proving Ground, MD, 1993.

27. Kaste, P. J.; Ceaser, J.; Lieb, R. J. *Scanning Electron Microscopy (SEM) to Probe Propellant Morphology*; ARL-TR-230; U.S. Army Research Laboratory: Aberdeen Proving Ground, MD, 1993.

28. MIL-DTL-398D. *RDX Detail Specification* **1996**.

29. von Allmen, M.; Blatter, A. *Laser-Beam Interactions With Materials: Physical Principles and Applications*, 2nd ed.; Springer-Verlag Berlin Heidelberg, New York, 2002.

30. Munson, C. A.; Gottfried, J. L.; De Lucia, F. C., Jr.; McNesby, K. L.; Miziolek, A. W. *Laser-Based Detection Methods for Explosives*; ARL-TR-4279; U.S. Army Research Laboratory: Aberdeen Proving Ground, 2007.

31. Nagura, C.; Suda, A.; Kawano, H.; Obara, M.; Midorikawa, K. Generation and Characterization of Ultrafast White-Light Continuum in Condensed Media. *Appl. Opt.* **2002**, *41* (18), 3735–3742.

| NO. OF COPIES | ORGANIZATION |
|---|---|
| 1 (PDF only) | DEFENSE TECHNICAL INFORMATION CTR<br>DTIC OCA<br>8725 JOHN J KINGMAN RD<br>STE 0944<br>FORT BELVOIR VA 22060-6218 |
| 1 | DIRECTOR<br>US ARMY RESEARCH LAB<br>IMNE ALC HRR<br>2800 POWDER MILL RD<br>ADELPHI MD 20783-1197 |
| 1 | DIRECTOR<br>US ARMY RESEARCH LAB<br>RDRL CIO LL<br>2800 POWDER MILL RD<br>ADELPHI MD 20783-1197 |
| 1 | DIRECTOR<br>US ARMY RESEARCH LAB<br>RDRL CIO LT<br>2800 POWDER MILL RD<br>ADELPHI MD 20783-1197 |
| 1 | DIRECTOR<br>US ARMY RESEARCH LAB<br>RDRL D<br>2800 POWDER MILL RD<br>ADELPHI MD 20783-1197 |

NO. OF COPIES ORGANIZATION

1 US ARMY RSRCH OFC
RDRL ROE N
R ANTHENIEN
PO BOX 12211
RSRCH TRIANGLE PARK NC 27709

1 US ARMY RSRCH OFC
RDRL ROP C
J PARKER
PO BOX 12211
RSRCH TRIANGLE PARK NC 27709

1 DARPA/DSO
J GOLDWASSER
3701 FAIRFAX DR
ARLINGTON VA 22203-1714

2 US ARMY AMRDEC
AMSRD AMR PS PT
J NEIDERT
P JOHNS
BLDG 7120
REDSTONE ARSENAL AL 35898

1 US ARMY ARDEC
AMSRD AAR AEE W
R DAMAVARAPU
BLDG 2028
PICATINNY ARSENAL NJ 07806-5000

3 US ARMY TACOM ARDEC
AMSRD AAR AEE W
R SURAPANENI
E BAKER
A DANIELS
BLDG 3022
PICATINNY ARSENAL NJ 07806-5000

1 US ARMY ARDEC
AMSRD AAR MEE W
S NICOLICH
BLDG 3022
PICATINNY ARSENAL NJ 07806-5000

1 US ARMY ARDEC
AMSRD AAR AEE W
E CARAVACA
BLDG 382
PICATINNY ARSENAL NJ 07806-5000

NO. OF COPIES ORGANIZATION

2 US ARMY ARDEC
RDAR MEE W
J O'REILLY
W BALAS-HUMMERS
BLDG 382
PICATINNY ARSENAL NJ 07806-5000

1 US ARMY TACOM ARDEC
V STEPANOV
BLDG 3028
PICATINNY ARSENAL NJ 07806-5000

1 US ARMY ARDEC
RDAR MEF E
D CARLUCCI
BLDG 94
PICATINNY ARSENAL NJ 07806-5000

1 US ARMY TACOM ARDEC
SFAE AMO CAS
P MANZ
BLDG 171A
PICATINNY ARSENAL NJ 07806-5000

1 US ARMY PEO AMMO
V MATRISCIANO
BLDG 171
PICATINNY ARSENAL NJ 07806-5000

1 NAVAL RSRCH LAB
TECH LIB
WASHINGTON DC 20375-5000

1 OFC OF NAVAL RSRCH
C BEDFORD
875 N RANDOLPH ST RM 653
ARLINGTON VA 22203-1927

2 NAVAL AIR WARFARE CTR
CODE 470000D
A ATWOOD
S BLASHILL
2400 E PILOT PLANT RD STOP 5001
CH1NA LAKE CA 93555-6107

1 NAVAL AIR WARFARE CTR
NAV AIR WEAPONS DIV
CODE 4T4320D
T PARR
1 ADMINISTRATION CIRCLE
CH1NA LAKE CA 93555-6100

NO. OF COPIES ORGANIZATION

2 DTRA
S PEIRIS
B WILSON
8725 JOHN J KINGMAN RD MS 6201
FORT BELVOIR VA 22060-6201

ABERDEEN PROVING GROUND

43 (39 HC 4 CD) US ARMY RSRCH LAB
RDRL CIO LA
T LANDFRIED (1 CD)
RDRL WML
M ZOLTOSKI
J NEWILL
RDRL WML A
F DE LUCIA (3 HC, 1 CD)
W OBERLE
RDRL WML B
J GOTTFRIED (3 HC, 1 CD)
S PIRAINO (3 HC, 1 CD)
J CIEZAK-JENKINS
J MORRIS
B RICE
W MATTSON
R PESCE-RODRIGUEZ
R SAUSA
N TRIVEDI
S BUNTE
RDRL WML C
K MCNESBY
K SPANGLER
B ROOS
E BUKOWSKI
M BISS
S AUBERT
RDRL WML D
R BEYER
RDRL WML E
P WEINACHT
RDRL WML F
D LYON
D HEPNER
RDRL WML G
W DRYSDALE
RDRL WML H
T BROWN
RDRL WMM
J ZABINSKI
RDRL WMP A
B RINGERS
RDRL WMP G
B HOMAN
N ELDREDGE

NO. OF COPIES ORGANIZATION

RDRL WM
B FORCH
P PLOSTINS
RDRL WM P
P BAKER